Computational Materials Science 212 (2022) 111598

Contents lists available at ScienceDirect

Computational Materials Science

journal homepage: www.elsevier.com/locate/commatsci

Full Length Article

Decoding crystal growth kinetics and structural evolution in supercooled ZnSe by molecular dynamics simulation

Leila Separdar [a,*], José Pedro Rino [a], Edgar Dutra Zanotto [b]

[a] Department of Physics, Federal University of São Carlos, Via Washington Luíz, km. 235, 13.565-905 São Carlos, SP, Brazil
[b] Department of Materials Engineering, Federal University of São Carlos, Via Washington Luíz, km. 235, 13.565-905 São Carlos, SP, Brazil

ARTICLE INFO

Keywords:
Crystal growth
Nucleation
Supercooled liquid
ZnSe
Molecular dynamics simulation
Seeding method

ABSTRACT

Crystallization is a vital process in nature and technology; however, the detailed microscopic mechanisms of crystal nucleation and growth in most materials and the associated theoretical models are still elusive. In this work, we applied molecular dynamics (MD) simulations of spontaneous and seeded growth to infer the crystallization kinetics in supercooled zinc selenide (ZnSe) liquid - used as a model material for which an excellent interatomic potential already exists. ZnSe is a type II-VI semiconductor with a wide bandgap. We determined the growth velocity, υ(T), in a range of temperatures and the structural evolution of both inserted and spontaneously formed nuclei. By determining υ(T) at shallow supercooling using the seeding method and extrapolating towards deep supercooling, where spontaneous nucleation and growth could also be detected by MD, we showed that the most probable growth mechanism in ZnSe and the related theoretical model is the Normal Growth (N-model). We also followed the growth kinetics dependency on the crystallographic orientation. The structure of the final crystal in both approaches, seeded and spontaneous growth, at different supercoolings, is a mixture of the two most stable phases of this material: zinc blende and wurtzite, with predominance of the latter. These results shed light on unknown aspects of crystal growth in this important supercooled liquid and indicate the best theoretical model (N-model), which could be further tested for other materials using the proposed approach - MD simulations of seeded combined with spontaneous crystallization.

1. Introduction

Crystal nucleation and growth are fundamental natural processes (e.g., snow and mineral formation), and central phenomena in technologies (e.g., metal solidification, single crystal synthesis, and glass–ceramic synthesis). Great effort has been made to study the fundamentals of crystal nucleation and growth in supercooled liquids (SCLs), with the overall aim of understanding the process and improving the control over the structure and resulting properties of single and polycrystalline materials produced from controlled crystallization (single crystals, metal alloys, and glass-ceramics). Crystal nucleation relies on the emergence of a critical nucleus from a SCL that enables other atoms or molecules to join the system, starting the second stage - crystal growth.

The growth kinetics of the crystalline nuclei precipitated inside a SCL have been studied in different types of materials, for example, experimentally in metal alloys [1,2,3], silicate glass-formers [4,5] and zeolites [6], and by computer simulations in ZrCu [7], Si [8], and water [9].

In the kinetic theory of crystal growth, the growth rate is expressed as the difference between the rate of molecular or atomic addition and subtraction to a crystal. According to classical theories, the growth rate can be separated into thermodynamic and kinetic terms. In deeply SCLs, the thermodynamic factor becomes constant and approaches unity, whereas the kinetic factor becomes increasingly slower as the temperature drops. Hence, determining this kinetic term is a necessary but challenging component to test growth theories. Based on the relationship between the thermodynamic and kinetic terms, two main theoretical models have been proposed to describe the crystal growth mechanism and dynamics. In the first model, which was proposed by Wilson [10] and Frenkel [11] (WF), the addition rate of atoms or molecules to a crystal is proportional to the atomic diffusion coefficient, $D(T)$, and the growth process depends on their mobility in the liquid phase, being a thermally activated process. In this model, which is called diffusion-controlled crystal growth, the rearrangement of the local liquid structure, such as reorientation of big molecules and bond breaking in network glasses, is necessary for an atom or molecule to

* Corresponding author.
E-mail address: separdar.leila@gmail.com (L. Separdar).

https://doi.org/10.1016/j.commatsci.2022.111598
Received 20 April 2022; Received in revised form 7 June 2022; Accepted 13 June 2022
Available online 22 June 2022

move or join the crystal; thus, there is a kinetic barrier for crystallization [12]. This model successfully describes the experimental crystal growth rates in various liquids, such as in elements (Ni [1], Ge [2], and Si [3]), alloys ($Zr_{50}Cu_{50}$ [7]), molecular liquids (o-terphenyl [13,14] and tri-α-naphthylbenzene [15]) and oxide glass-formers (Li_2O-$2SiO_2$ [16], B_2O-$2SiO_2$ [4], and CaO-MgO-$2SiO_2$ [17]); and by computer simulations in $Zr_{50}Cu_{50}$ [18], $K_2O.SiO_2$ [19], $Ni_{50}Ti_{50}$ [20] alloy, and Ag [21].

Unlike the WF model, in the second scenario, which was proposed by Broughton-Gilmer-Jackson (BGJ) [22], called collision-controlled crystal growth, the ordering kinetics is controlled by the thermal velocity of the particles, $\sqrt{3k_BT/m}$, where m is the atom mass and k_B is the Boltzmann constant. In this model, there is no energy barrier to the motion of an atom across the liquid/crystal interface and no need to rearrange the local structure of the liquid for crystallization. This diffusionless growth model describes well the experimentally measured crystal growth velocities of colloidal systems at deep supercooling [23], and provides a reasonable fit to the experimental crystal growth velocity of Ag at shallow supercooling [33]. It also describes quite well the simulation results of the crystallization rates in Lennard-Jones liquid [22] and simple metals and alloys, such as Ni [24], Cu [24], Na [25], Mo [26], Au [27], Fe [28], Co [29], $Cu_{50}Ni_{50}$ [30], Pt [31], and Ni_3Al [32].

However, these theories fail for other substances, or are valid only in a certain range of undercooling. For instance, at deep supercooling, the WF model underestimates the growth rates obtained from simulations for pure elements such as Ta, Va, Pt [31], and Ag [33], whereas for multicomponent alloys, both theoretical descriptions (WF and BGJ) overestimate the growth rates [18,34,35,36]. Hence, which model best describes crystal growth rates in different substances in a wide temperature range is still elusive, and demands further study.

When dealing with crystal growth, the crystallographic dependence of growth velocity is important. In most materials, the crystallization velocity depends on the front orientation, for example, in the case of Ag [21] crystallization proceeds faster at the [1 0 0] than at the [1 1 0] and [1 1 1] orientations.

Considering the aforementioned issues, in this paper, we study the crystal growth mechanism in SCL zinc selenide (ZnSe) from both the overall kinetics and crystallographic perspectives. ZnSe was chosen because a reliable interatomic potential is available for its simulation, which can correctly describe mechanical, thermodynamical and structural phase transformations, as well as spontaneous crystallization at deep supercooling. This potential was proposed by one of us (J.P. Rino) [37], and we successfully investigated its nucleation stage (not growth) [38]; hence, we already have great confidence in it. Also, ZnSe is very important in optics [39,40]. It is a type II-VI semiconductor with a wide bandgap that can be made in both hexagonal (wurtzite) and zinc-blende (cubic) structures. Experimental attempts have been made to understand its structural evolution and crystallization from vapor and melt [41,42,43]. Hence, knowledge about its crystal growth mechanism is significant for technology applications.

Among different techniques, seeded growth is an efficient way to promote the formation and growth of critical nuclei and to control the crystal size distribution [44,45,46,47,48,49]. Seed crystals provide a substrate for the desired product to nucleate and grow, thus replacing self-generation in seed-free processes. In our previous works, we have used a combination of seeding and spontaneous crystallization to study the nucleation process in ZnSe [38] and BaS [50]. By this method, we have determined the critical nucleus sizes, the atomic transport coefficient at the nucleus/liquid interface, and the interfacial free energy at shallow supercooling. The extrapolated growth rates to deep supercooling using the Classical Nucleation Theory (CNT) agreed quite well with the values obtained directly by molecular dynamics (MD) simulations (at deep supercoolings) via the mean lifetime method [38]. These results confirmed the ability of the seeding method to estimate nucleation parameters and the applicability of the CNT.

In this article, we intend to take one step forward and use the seeding method to find the growth velocities at sallow supercooling in ZnSe (where the spontaneous formation of crystalline nuclei does not occur in MD time scales), and extrapolating them with the WF and BGJ theories toward deep supercooling. Then we will compare the growth velocities calculated from these theories with those obtained with spontaneous nucleation and growth at deeper supercoolings. By this procedure, a wide range of temperatures will be covered to check the applicability of available crystal growth models over the whole temperature range, from shallow to deep supercoolings. Overall, we aim to understand the structural evolution and growth mechanism in ZnSe.

The paper is organized as follows: Section 2 presents the classical theoretical equations used to describe crystal growth. In Section 3, the simulation details are explained. Section 4 is devoted to discuss the MD results and tests of the theories. Finally, Section 5 presents our conclusions.

2. Basic equations and theoretical models

As mentioned in the Introduction section, the steady-state crystal growth velocity, $v(T)$, is described theoretically as the difference between the rate of atomic addition and subtraction to a crystal. By invoking microscopic reversibility, this difference can be separated into a thermodynamic term, $1-exp(-|\Delta\mu(T)|/k_BT)$, and a kinetic term, $k(T)$:

$$v(T) = k(T)[1 - exp(-\Delta\mu(T)/k_BT)], \tag{1}$$

where k_B is the Boltzmann constant. The thermodynamic driving force, $\Delta\mu$, is the difference between the crystal and liquid chemical potentials, $\Delta\mu = \mu_{cry} - \mu_{liq}$.

2.1. Theoretical models

Two main theories regarding the temperature dependence of $k(T)$ are the diffusion-controlled and collision-controlled growth mechanisms. In the first one, known as the Wilson-Frenkel (WF) setting [10,11], the kinetic term is governed by diffusion,

$$k(T) = \frac{fCLD(T)}{\lambda^2} \tag{2}$$

where $D(T)$ is the diffusion coefficient of the atomic species in the bulk SCL, which controls atomic attachment at the liquid/crystal interface. For a binary substance (ZnSe, in our case), we will take the average between the diffusion coefficients of the two types of atoms. λ is a diameter of the diffusing particle, which is equal to jump distance, and is related to the position of the first peak in the radial distribution function. The ratio λ^2/D corresponds to the average time required for a particle to diffuse a distance of one diameter, which will be referred to as diffusion time. The crystallographic dependence of growth velocity is reflected into the theory through the parameter L, which is the crystal lattice spacing. In general, λ is very similar to L. f is the fraction of preferred growth sites at the interface, and its value depends on the growth mechanism. C is the rate of addition of layers per diffusion time after factoring out the reverse process contribution to the dynamics. This unitless parameter C is obtained from fitting.

In the theoretical model proposed by the Broughton-Gilmer-Jackson (BGJ) [22], the atomic addition rate is proportional to the thermal velocity of the atoms (particles).

$$k(T) = (fCL/\lambda)\sqrt{\frac{3k_BT}{m}} \tag{3}$$

where m is the particle mass.

Returning to the WF setting, two main growth modes exist: one is the "Continuous" or "Normal" growth model (N-model), and the second is the "Screw Dislocation" model (SD-model). In the N-model, the crystal surface is atomically rough, and the degree of roughness is not temperature dependent; hence, $f \approx constant \approx 1.0$. In the SD-model, the

crystal/SCL interface is smooth on the atomic scale, and atomic or molecular addition to a growing crystal may occur preferentially on screw dislocations [51], with a fraction $f << 1$ on the crystal surface, which is given approximately by the Uhlmann [52,53] expression, $f \cong \frac{(T_m - T)}{2\pi T_m}$, where T_m is the melting temperature. Finally, when the crystal/SCL interface is defect-free, there is still another mechanism, called the 2*D* or secondary surface nucleated growth model [54], which will not be further discussed here because it is quite rare.

We will check these scenarios of crystal growth in supercooled ZnSe crystallized by the seeding and spontaneous approaches to test whether one of them describes the growth velocities obtained directly from spontaneous nucleation at deep supercooling. For the analytical estimates, we will express the thermodynamic driving force in its widely used form [55],

$$\Delta\mu = \Delta h_m \frac{(T_m - T)}{T_m} \tag{4}$$

where Δh_m is the difference in the enthalpy of the crystal and liquid at the melting point (heat of melting). In the case of ZnSe, $T_m \cong 1388K$ and $\Delta h_m = 0.266ev/atom$ [38]. This expression is valid when the difference between the specific heats of the crystal and the SCL is very small, and thus gives an upper bound for $\Delta\mu$.

3. Details of the simulation

In the seeding method, a crystalline cluster of a certain size is artificially inserted into a SCL. The procedure of inserting the seed in ZnSe was described in detail in our previous work on crystal nucleation [38]. The procedure can be summarized as follows: we started with an equilibrated crystal of ZnSe with a zinc-blende (ZB) structure at T = 300 K, heated it up to T = 1000 K, and then defined a spherical region in the center of a hot crystalline matrix. Hence, initially, the spherical seed and surrounded matrix had the same structure and lattice parameters. After that, only the solid matrix was heated up to T = 2000 K to liquefy and then quenched down to T = 1000 K. During the cooling process, the seed was released at different temperatures to verify which one was the seed/SCL coexistence temperature. Because the seed atoms inside the spherical region were held fixed at their positions, they experienced a certain strain. To remove this strain, after releasing the seed at each given temperature, we first let the thermostat and barostat remove this strain by controlling the temperature and pressure of both the seed and the supercooled liquid, and only then investigated the seed growth.

To study the seed growth, extensive MD simulations have been conducted for three systems composed of 17,576, 32,768 and 64,000 atoms in cubic boxes of $L_x = L_y = L_z = 73.36A^\circ, 98.34A^\circ$ and $112.86A^\circ$, respectively. The interactions between the atoms were modeled by a reliable potential described in Refs. [37,38]. Simulations were performed at constant pressure ($p = 0bar$) in an NpT ensemble using the LAMMPS package [56]. The timestep was $1.0fs$. The Nosé-Hoover thermostat and barostat were used to control the temperature and pressure, respectively. Periodic boundary conditions were applied in all directions. Four seed sizes with radii $r = 13, 11, 9.5$and$8.5A^\circ$ were inserted into supercooled ZnSe separately, and their size evolutions were monitored over time. For reliable statistics, 10 independent configuration samples of the matrix containing the same nucleus size were studied. In this way, the seed structure and kinetics during its growth path were analyzed in detail, and are described in the next section.

4. Results

4.1. Growth velocity

4.1.1. Seeding experiments

Determining the seed/SCL coexistence temperature, T^*, is the first step to study their growth. Because the equilibrium between the crystalline seed and the surrounding metastable liquid could demand a very long simulation time to be reached, we defined the coexistence temperature as that at which the seed grows and stabilizes in five or six out of ten independent configurations and fully dissolves in the remained configurations. A good criterion to determine the growth of a crystalline seed is looking at the time evolution of the potential energy or enthalpy. A sharp decrease in potential energy indicates seed growth and the beginning of a phase transition. If it increases or remains approximately unaltered, this means that the seed has dissolved. We determined the coexistence temperatures for four seed sizes by monitoring the potential energy over the initial $0.5ns$. The results are shown in Table 1. After determining T^* for each seed size, the systems where the seed grows were let to evolve for extra $2.5ns$.

Fig. 1(a) shows the time evolution of the number of solid-like atoms, N^*, in five of ten independent configurations at $T^* = 1220 \pm 5K$ in the system composed of 64,000 atoms containing a seed with $r = 13A^\circ$. The seed fully dissolved in the remained configurations. Solid-like (crystalline) particles in the seed environment were identified by calculating the Steinhardt bond-order parameter [57,58], $S_{ij} = \sum_{m=-6}^{m=+6} q_{6m}(i).q^*_{6m}(j)$, where $q_{6m}(i) = \frac{1}{N_b(i)}\sum_{j=1}^{N_b(i)} Y_{lm}(\overrightarrow{r}_{ij})$ is the Steinhardt parameter, $Y_{lm}(\overrightarrow{r}_{ij})$ are the spherical harmonics, $N_b(i)$ is the number of nearest neighbors of atom i, and $\overrightarrow{r}_{ij}$ is the vector connecting it with its neighbors j. If the value of the dot product $q_6.q^*_6 > 0.5$, the particle–particle association was considered solid-like. We tested the q_6 results using a set of different numbers of connections at one temperature to find out which one is the most appropriate for the crystallization case. In this case, if a particle was involved in more than 11 solid-like associations, we considered that it was in the (crystal) seed environment. This number agrees with the coordination number calculated from the area under the first peak of the radial distribution function [37]. Knowing N^* and assuming a spherical shape for the seed (although this is not perfectly true), the seed radius, r, was calculated using the crystal number density at T^* via the relation $\rho_{crystal}(T^*) = 3N^*/(4\pi r^3)$. Fig. 1(b) displays the time evolution of r for the configurations shown in Fig. 1(a). In Fig. 1(c), the effect of the system size on the growth path is demonstrated. As shown, seed growth proceeds via three stages in this system. The first stage relates to a time interval, Δt_1, at which the seed starts to grow until it reaches the second stage. In the second stage, crystal growth continues with constant velocity for a time interval Δt_2. This time interval varies for each configuration and strongly depends on the system size; it increases by increasing the box size. After this stage, for a time interval Δt_3, growth stops because of the limited system size. As demonstrated in Fig. 1(c), for the smallest system size, seed growth has been halted by its periodic image before entering the steady-state growth regime. Doubling the system size from 17,568 to 32,768 atoms causes the steady-state stage of crystal growth to become distinguishable from the two other stages. However, for better statistics and more reliable results, we doubled this system size again. Increasing even more the system size would not change the growth velocity. The radial growth velocity was determined by a linear fit to the data in this intermediate regime. The average velocity obtained for a seed with $r = 13A^\circ$ over five independent configurations is $v = \dot{r} = 0.050 \pm 0.002A^\circ/ps$. Henceforth, we will only report results related to the largest box size.

The same calculations and analyses were carried out for three other seed sizes with radii $r = 11, 9.5and8.5A^\circ$. Table 1 shows the growth velocity obtained for each seed size.

4.1.2. Spontaneous nucleation and growth at deep supercoolings

We have shown previously that in the deep supercooling regime, i.e., $T = (0.61 - 0.72)T_m$, ZnSe crystalizes spontaneously in MD time scales [38]. Therefore, we can also obtain the growth velocity in this region without inserting a seed. To this end, starting from liquid ZnSe at $T = 2000K$, which is above the melting point, we cooled the system at a fast

Table 1
Growth velocity, $v(T)$, of the inserted seed with different radii, r, at the seed/SCL coexistence temperature (T^*)

$r(A^\circ)$	13	11	9.5	8.5
$T^*(K)$	1220	1210	1155	1130
$v(T)(A^\circ/ps)$	0.050 ± 0.005	0.0514 ± 0.005	0.0676 ± 0.005	0.071 ± 0.004

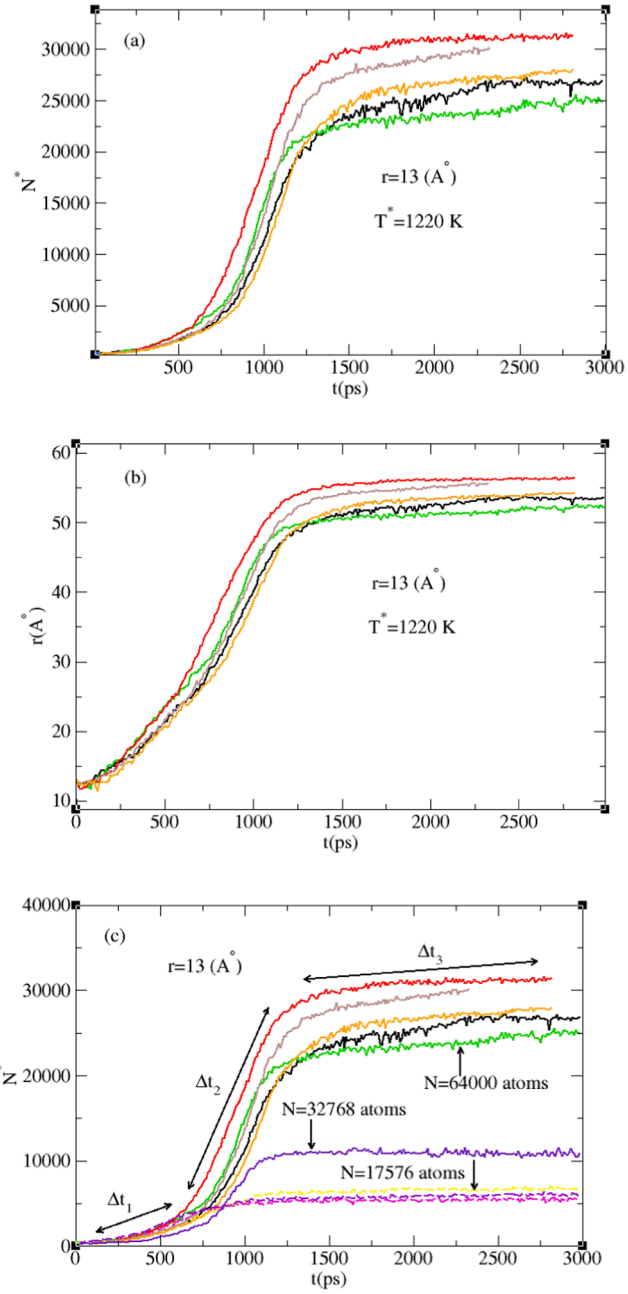

Fig. 1. Time evolution of (a) the number of solid-like atoms and (b) seed radius growth in the system composed of 64,000 atoms containing a seed with $r = 13A^\circ$. The curves in each plot refer to those configurations in which the seed grows. (c) Time evolution of the number of solid-like atoms in systems with 17,576, 32,768 and 64,000 atoms containing a seed with $r = 13A^\circ$. The steady-state stage of crystal growth related to time interval, Δt_2, which depends on the system size.

rate, $1K/ps$, down to $T = 1000, 950$ and $900K$. Then the ZnSe SCL was let to evolve for $3ns$ at each temperature, and the number of solid-like atoms was counted using the Steinhardt bond-order parameter criterion, as previously explained. From the evolution of the total number of solid-like atoms, we calculated the growth rates. For reliable statistics at each temperature, 10 independent configurations were studied and the growth rates were averaged over them.

A fit to the growth rate data obtained from the seeding procedure, according to the WF and BGJ models, and extrapolating the resulting expression to deep supercooling to compare them with the spontaneous growth velocities, could show which theory best describes the growth kinetics over the whole temperature range. The fitting and extrapolation procedure is as follows: In the framework of the WF setting, according to Eq. (2), one needs to know the self-diffusion coefficient ,$D(T)$, and the factor C for the desired extrapolation. $D(T)$ was obtained by computing the mean-square displacements via the Einstein relation, $\langle r^2(t)\rangle = 6Dt$, for the two elements in the temperature range, $1000K < T < 1600K$, shown in Fig. 2. The resulting diffusion coefficients can be reasonably fitted using the Arrhenius expression,

$$D(T) = D_0 \exp\left(-\frac{E_A}{K_B T}\right) \tag{5}$$

down to $T = 1100$K; for lower temperatures, the Arrhenius expression overestimates the actual data. The activation free energies are $E_A = 0.60eV$ for Zn and $E_A = 0.73eV$ for Se. The pre-exponential factors are $D_0 = 53.9A^{\circ 2}/ps$ for Zn and $D_0 = 108.54A^{\circ 2}/ps$ for Se. Fig. 2 represents the Arrhenius-type plot of $D_{Zn}(T)$, $D_{Se}(T)$, and their average $D_{avg}(T) = (D_{Zn}(T) + D_{Se}(T))/2$ in conjunction the Arrhenius fits.

To determine the factor C, we used Eqs. (1) and (2) in the framework of the WF setting and rescaled the growth velocity as.

$$v(T)\lambda^2/fLD(T) = C[1 - exp(-\Delta\mu(T)/k_B T)] \tag{6}$$

by substituting the values of v, $\lambda = 2.5A^\circ$(the position of the first peak of the radial distribution function of Zn-Se pairs), the D_{avg} at each T^*, and the $\Delta\mu$ from Eq. (4). Fig. 3 (a) and (b) show $v(T)\lambda^2/LD(T)$ as a function of $1 - exp(-|\Delta\mu(T)|/k_B T)$ for the N- and SD-models with $f = 1$ and $f \cong \frac{(T_m - T)}{2\pi T_m}$, respectively. A linear relationship, demonstrating that the expression presented in Eq. (6) has indeed successfully captured it.

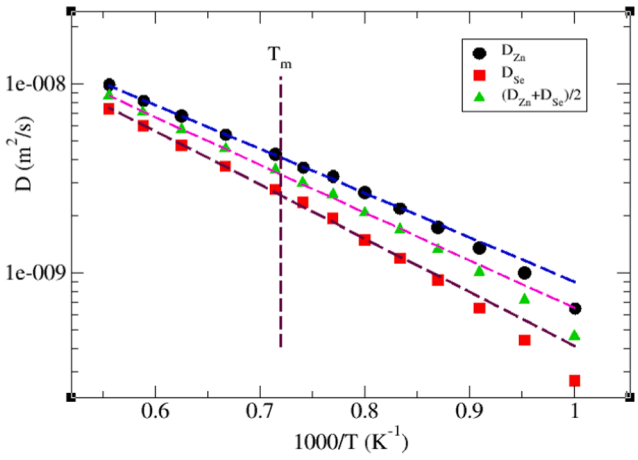

Fig. 2. Arrhenius plot of the simulated translational diffusion coefficient, $D(T)$, in ZnSe obtained from the mean squared displacements via the Einstein relation. The dashed lines are fits to the Arrhenius expression (Eq. (5)). Please note that the data move away from the Arrhenius lines at the lowest temperatures, $T < 1100K$.

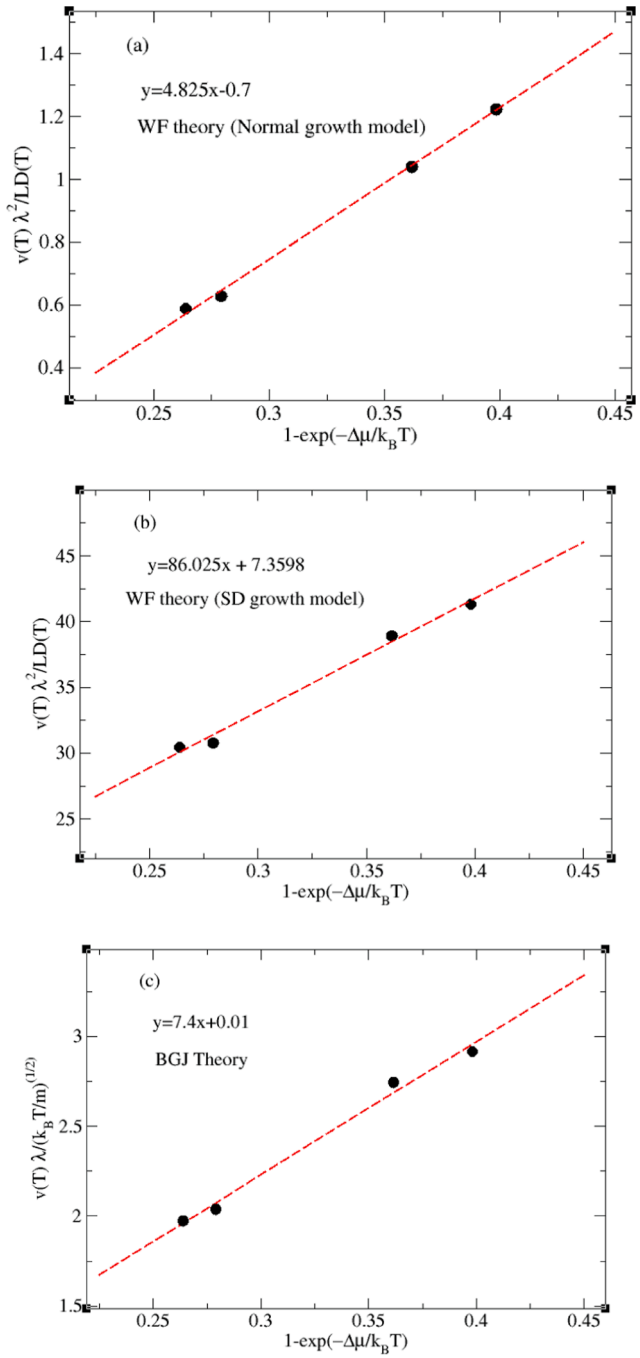

Fig. 3. Reduced growth rates, as described in the text (Eqs. (6) and (7)). The red lines correspond to linear fits according to (a) the WF theory with the N-model, (b) the WF theory with the SD-model, and (c) the collision-controlled growth mechanism (BGJ theory).

The values of C are 4.82 and 86.03 for the N- and SD-models of the WF theory, respectively. Knowing the temperature depended on $D(T)$ and C, we extrapolated the data toward deep supercooling, which is demonstrated by the black, blue and red lines in Fig. 3.

Using Eqs. (1) and (3) in the framework of the BGJ theory, the rescaled velocity is.

$$\frac{\lambda v(T)}{L\sqrt{\frac{3k_BT}{m}}} = C[1 - \exp(-\Delta\mu(T)/k_BT)]. \tag{7}$$

Fig. 3 (c) shows $v(T)/\sqrt{k_BT/m}$ *vs.* $1 - exp(-|\Delta\mu(T)|/k_BT)$. The linear relation shows that this setting is also able to describe the growth rates obtained from the seeding method at shallow supercooling. A linear fit to data gives the factor C. The value of C, obtained from the slope in Fig. 3 (a) for the N-model is 4.82. This value is comparable to those obtained for a NiAl alloy, which is 5.3, and 3.5 for the [1 0 0] and [1 1 0] surfaces, respectively. This value is 0.4 for the good glass former CuZr and 0.3 for analogous surfaces [18], respectively; thus, our result is in the same order of magnitude.

Finally, by knowing C, we are able to extrapolate the expression to deep supercooling, which is shown by the red dashed line in Fig. 4. The difference between these two theoretical expressions becomes clear at deeper supercooling. The best result is provided by the N-model. Also, according to the Jackson's criterion of crystal growth, based on the description of the crystal/melt interface structure [53,59], the melting entropy of the ZnSe crystal is relatively small: $\Delta S_m = \frac{\Delta h_m}{T_m} \cong 2R$ (R is the gas constant), which confirms that the Normal growth mechanism should prevail for ZnSe.

As shown by experiments [33], a maximum in $v(T)$ is predicted, which is a consequence of the competition between opposing thermodynamic and kinetic effects. This maximum occurs at $(0.6 - 0.8)T_m$ for metals and at $(0.90 - 0.98)T_m$ for oxide glass-formers [60]. For most substances, this maximum occurs at a temperature range between the melting and glass transition. Fig. 4 captures this feature. For the N- and SD-models, the maxima occur at $T_{v_{max}} = 0.79T_m$ and $T_{v_{max}} = 0.75T_m$ respectively, which are above the glass transition temperature, $T_g = 0.57T_m$, of ZnSe for the particular cooling rate used here. A previous work found that for a diversity of glass-forming systems, $\frac{T_{v_{max}}}{T_g} = 1.48 \pm 0.15$ [61]. For ZnSe, this value is quite close: $\frac{T_{v_{max}}}{T_g} = 1.41 \pm 0.02$. In the case of the BGJ theory, in the region of deep supercooling, the growth velocity increases monotonically up to $T_{v_{max}} = 0.51T_m$, which is lower than T_g, and then starts to decrease. This maximum is shown in Fig. 4.

4.2. Crystal structure

It is known that nucleation is a control factor in fixing the crystal structure, e.g., [62]. Hence, it is important to compare the final structure of the crystal crystalized by seeding with that of the spontaneously nucleated crystal. In this section, the crystal structures are investigated and compared. Fig. 5 shows the time evolution of a seed cross-section area with $r = 13A^{\circ}$ at $t = 0, 0.5, 1, 1.5, 2.0$and$3.0ns$ from left to right,

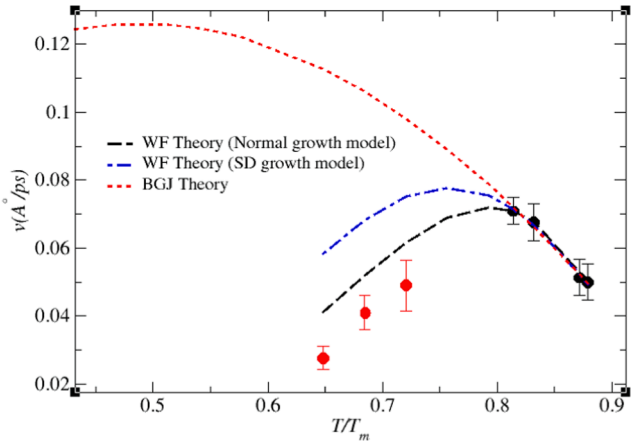

Fig. 4. Temperature dependence of the average crystal growth velocity in supercooled ZnSe. The black circles display the average growth velocity obtained from the seeding method and the red circles refer to the average growth velocity obtained from spontaneous nucleation at deep supercoolings. The black, blue and red dashed lines refer to fittings and extrapolations of $v(T)$ using the "Normal" and the "Screw Dislocation" diffusion-controlled crystal growth (WF theory) settings (Eq. (2)) and the collision-controlled growth mechanism (BGJ theory) setting (Eq. (3)), respectivly.

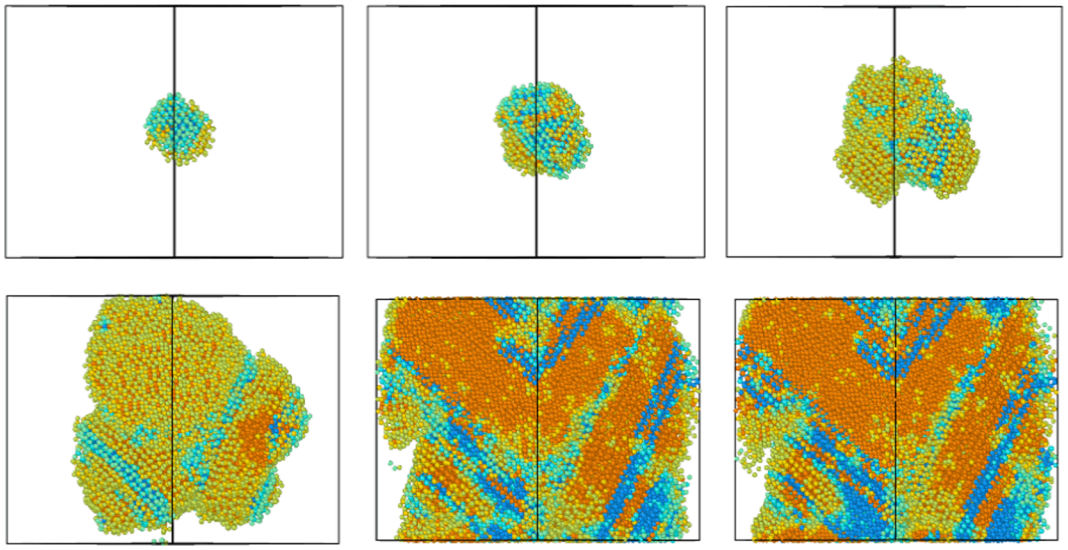

Fig. 5. Snapshots of the time evolution of the seed cross-section area with $r = 13A^{\circ}$ at $t = 0, 0.5, 1, 1.5, 2.0 and 3.0 ns$ from left to right, respectively, in the crystallographic direction [1 1 0]. The blue atoms have the ZB structure and the others have the WZ structure.

respectively, in the crystallographic direction [1 1 0]. This direction clearly shows the formation of the ZB and wurtzite (WZ) layers. During the growth procedure, the first layer formed on the initial lattice structure of seed (ZB), has the WZ structure. At longer times, layers with the ZB structure also form on the WZ layers, and are shown in blue in Fig. 5. The WZ growth on ZB was previously reported in Ref. [63]. This preference for growth and alternation of WZ and ZB is also observed in the crystal produced through spontaneous nucleation at deep supercooling, and can be associated with the relatively small difference in the total energy between these two structures, which experimentally is only $5.3 meV/atom$ [64]. In our simulation, this energy difference is approximately $8 meV/atom$ [37].

As discussed in the Introduction, growth velocity is affected by front orientation. We have examined this direction dependency and measured the inserted seed areas with radii $r = 8.5A^{\circ}$ and $r = 13A^{\circ}$ in the [1 0 0], [0 1 0], [0 0 1], [1 1 0] and [1 1 1] directions using the Fiji software [65]; the results are shown in Fig. 6. The dashed lines relate to a system containing a seed of $r = 8.5A^{\circ}$ and the solid lines refer to a system containing seed of $r = 13A^{\circ}$. From this figure it can be inferred that the seed grows faster in the direction [1 1 1] than in other directions, whereas the growth rate in the directions [1 0 0], [0 1 0] and [0 0 1] are

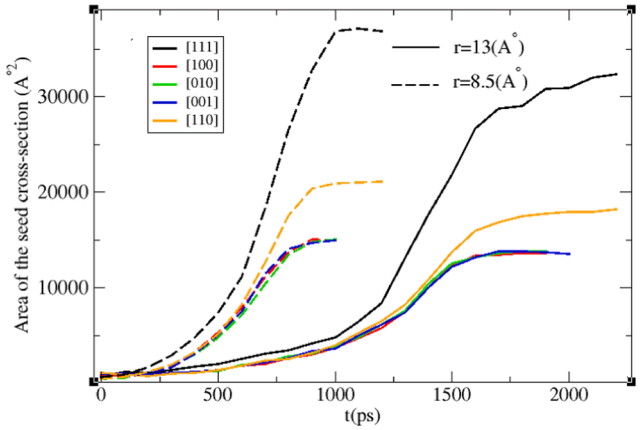

Fig. 6. Time evolution of a seed cross-section area in different crystallographic directions for two systems containing seeds with radii $r = 13A^{\circ}$ (solid lines) and $r = 8.5A^{\circ}$ (dashed lines). The relative growth velocities are $v_{[111]} \approx 2v_{[110]} \approx 2v_{[100]}$ and $v_{[100]} = v_{[010]} = v_{[001]}$.

the same, $v_{[100]} = v_{[010]} = v_{[001]}$. Hence, the related growth velocity curves fall on top of each other. The relative growth velocities are $v_{[111]} \approx 2v_{[110]} \approx 2v_{[100]}$. It should be mentioned that the growth of WZ and ZB layers follow the same crystallographic direction as [1 1 1].

Fig. 7(a) shows the time evolution of the total radial distribution function for the SCL crystalized by seeding at some selected times after inserting the seed with radius $r = 13A^{\circ}$. A comparison was conducted between 1) the structure of the system crystallized by inserting the seed after $3 ns$, 2) the crystalline system with ZB and WZ structures at $T = 1220K$, and 3) the structure of the system that spontaneously nucleated at $T = 900K$ after $3.0 ns$. The structure of the system crystallized by seeded nucleation is similar to that of the system spontaneously nucleated; however, the structure of the system by inserting the seed after $3 ns$ is not exactly ZB or WB because of the formation of layers with varying structures around the seed. For $r < 5.5A^{\circ}$, the system structure is more similar to WZ. There is a thermal broadening and, also, ZB and WZ are very similar at small distances; however, for $r > 5.5A^{\circ}$, there is a deviation from the WZ structure. It is worth noting that layers with different structures have also been reported in simulations of homogeneous nucleation and growth of Al [45], BaS [66], and Cu [67]. Hence, as suggested from experiments [68], seeding with the desired crystalline structure (here the ZB structure) is not sufficient to ensure the growth of this crystalline structure.

5. Conclusions

In this work, we investigated the crystal growth mechanism and dynamics in supercooled ZnSe. This semiconductor is a poor glass former with the ability to nucleate spontaneously at temperatures $T < 0.75T_m$. By taking advantage of this property, we obtained growth velocities at deep supercooling directly from the simulations. We also obtained growth velocities at shallow supercooling using the seeding method, thus covering a wide temperature range.

A comparison between the extrapolated growth rates from shallow to deep supercooling with values obtained directly from spontaneous nucleation and growth (at deep supercooling) showed that the best theoretical model for this material is the "Normal" (diffusion-controlled) crystal growth. However, as the diffusion coefficient follows an Arrhenius behavior at shallow supercooling down to $T = 1100K$ but a deviation is observed at deep supercooling, the use of extrapolated $D(T)$ overestimates the calculated growth velocities in this temperature range. Such overestimate by the WF model has been previously observed

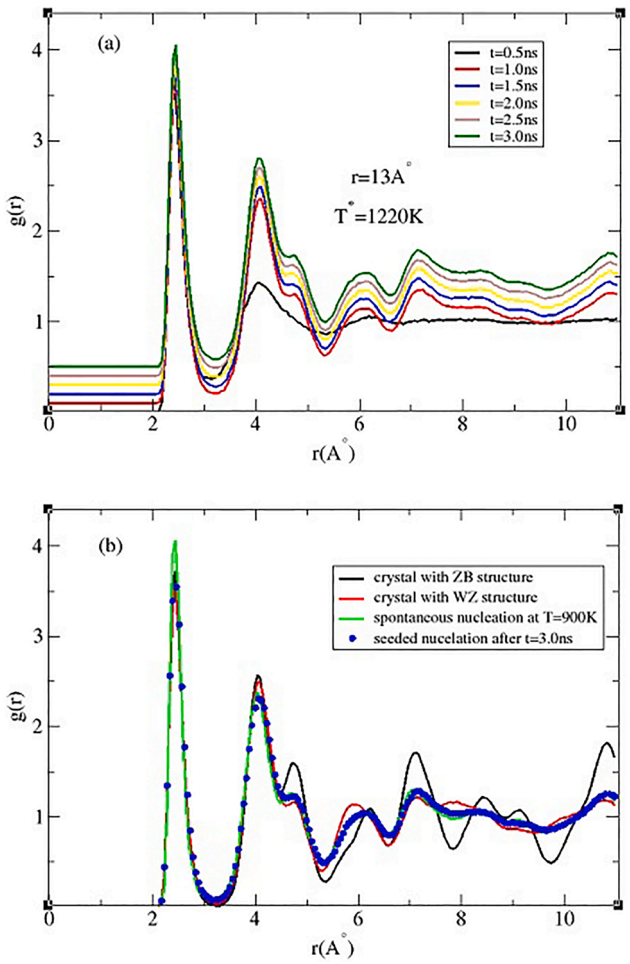

Fig. 7. (a) Time evolution of the radial distribution function of the Zn-Se pair in the system containing seed with $r = 13A^{\circ}$ at$T^{*} = 1220K$. Each curve has been shifted by $0.1n(n = 1, 2, 3\cdots)$ for clarity; (b) comparison between the structure of the seed + matrix system after 3*ns* with the structure of the crystalline system at the same temperature with two possible structures, i.e., ZB and wurtzite, and the system that spontaneously nucleated and evolved for 3 *ns*.

in multicomponent alloys [34,35,36].

After the whole system crystallizes via seeding at shallow supercooling, the crystal structure is very similar to that produced through spontaneous nucleation at deep supercooling. Although the inserted seed had a zinc-blende structure, which is the most stable polymorph of ZnSe, during the growth process layers with wurtzite structure also form, which demonstrates that seeding with the desired crystalline structure (here the ZB structure) does not always lead to the same crystalline structure. It is relevant to stress that, even in the case of spontaneous nucleation, a mixture of zinc-blende and wurtzite was observed. This double-crystal formation probably occurs because the difference in the thermodynamic stability of the two phases is quite small.

Overall, the combination of seeding and spontaneous crystallization proved to be a good method to evaluate growth rates in wide temperature ranges and the structure of the resulting crystals. These results unveil unknown aspects of crystal growth in this important semiconductor and indicate the best theoretical expression (N-model), which can now be further tested for other materials using our MD approach.

CRediT authorship contribution statement

Leila Separdar: Formal analysis, Investigation, Writing – original draft, Writing – review & editing, Visualization, Funding acquisition. **José Pedro Rino:** Conceptualization, Methodology, Validation, Writing – review & editing, Supervision, Project administration. **Edgar Dutra Zanotto:** Validation, Formal analysis, Writing – review & editing, Supervision, Project administration.

Declaration of Competing Interest

The authors declare that they have no known competing financial interests or personal relationships that could have appeared to influence the work reported in this paper.

Data availability

All the data used in this study can be made available to any interested reader upon request to the authors.

Acknowledgement

We would like to thank CNPq, Brazil, and the São Paulo Research Foundation, FAPESP, Brazil (contract Cepid no. 2013/007793-6) for funding this work, and for a postdoctoral fellowship to LS (grant no. 2019/09499-4).

References

[1] O. Funke, G. Phanikumar, P.K. Galenkoa, L. Chernova, S. Reutzel, M. Kolbe, D. M. Herlach, Dendrite growth velocity in levitated undercooled nickel melts, J. Cryst. Growth 297 (2006) 211.
[2] S.E. Battersby, R.F. Cochrane, A.M. Mullis, Highly undercooled germanium: growth velocity measurements and micro structural analysis, Mater. Sci. Eng. A 226 (1997) 443.
[3] C. Panofen, D.M. Herlach, Solidification of highly undercooled Si and Si–Ge melts Mater, Sci. Eng. A 669 (2007) 449.
[4] A.M. Rodrigues, D.R. Cassar, V.M. Fokin, E.D. Zanotto, Crystal growth and viscous flow in barium disilicate glass, J. Non-Crystal. Solids 479 (2018) 55.
[5] M.L.F. Nascimento, E.D. Zanotto, Mechanism and dynamics of crystal growth, viscous flow, and self-diffusion in silica glass, Phys. Rev. B 73 (2006), 024209.
[6] J. Grand, H. Awala, S. Mintova, Mechanism of zeolites crystal growth: new findings and open questions, Cryst. Eng. Comm 18 (5) (2016) 650–664.
[7] Q. Wang, et al., Diffusion-controlled crystal growth in deeply undercooled $Zr_{50}Cu_{50}$ melt on approaching the glass transition, Phys. Rev. B. 83 (2011), 014202.
[8] P. Keblinski, Thermodynamics and kinetics of melting and growth of crystalline silicon clusters, MRS Proceedings 536 (1998) 311.
[9] F. Leoni, R. Shi, H. Tanaka, J. Russo, Crystalline clusters in mW water: stability, growth, and grain boundaries, J. Chem. Phys. 151 (2019), 044505.
[10] H.A. Wilson, On the velocity of solidification and viscosity of super-cooled liquids, Philos. Mag. 50 (1900) 238.
[11] J. Frenkel, On the electric and photoelectric properties of contacts between a metal and a semiconductor, Phys. Z. Sowjetunion 1 (1932) 498.
[12] K.A. Jackson, The interface kinetics of crystal growth processes, Inter Sci. 10 (2002) 159.
[13] R.J. Greet, J.H. Magill, An empirical corresponding-states relationship for liquid viscosity, J. Phys. Chem. 71 (1967) 1746.
[14] D.J. Plazek, C.A. Bero, I.-C. Chay, The recoverable compliance of amorphous materials, J. Non-Cryst. Solids 172-174 (1994) 181–190.
[15] J.H. Magill, D.J. Plazek, Physical Properties of Aromatic Hydrocarbons. II. Solidification Behavior of 1, 3, 5-Tri-α-Naphthylbenzene, J. Chem. Phys. 46 (1967) 3757.
[16] T. Fuss, A. Moguš-Milanković, C.S. Ray, C.E. Lesher, R. Youngman, D.E. Day, Ex situ XRD, TEM, IR, Raman and NMR spectroscopy of crystallization of lithium disilicate glass at high pressure, J. Non-Crystalline Solids 352 (2006) 4101.
[17] V.M. Fokin, M.L.F. Nascimento, E.D. Zanotto, Correlation between maximum crystal growth rate and glass transition temperature of silicate glasses, J. Non-Cryst. Solids 351 (10-11) (2005) 789–794.
[18] C. Tang, P. Harrowell, Anomalously slow crystal growth of the glass-forming alloy CuZr, Nat. Mater. 12 (2013) 507.
[19] G.W. Scherer, D.R. Uhlmann, Diffusion-controlled crystal growth in $K_2O.SiO_2$ compositions, Journal of Non-Crystalline Solids 23 (1977) 59.
[20] S. An, Y. Li, J. Li, S. Zhao, B. Liu, P. Guan, The linear relationship between diffusivity and crystallization kinetics in a deeply supercooled liquid Ni50Ti50 alloy, Acta Mater. 152 (2018) 1.
[21] G.M. Poletaev, Y.V. Bebikhov, A.S. Semenov, R. Yu Rakitin, Molecular dynamics study of the influence of supercooling temperature and orientation of the crystallization front on its velocity in silver, J. Phys. Conf. Ser. 2131 (4) (2021) 042053.
[22] J.Q. Broughton, G.H. Gilmer, K.A. Jackson, Crystallization rates of a Lennard-Jones liquid, Phys. Rev. Lett. 49 (1982) 1496.

[23] Q. Gao, J. Ai, et al., Fast crystal growth at ultra-low temperatures, Nature Materials 20 (2021) 1431.
[24] J.J. Hoyt, B. Sadigh, M. Asta, S.M. Foiles, Atomistic simulation methods for computing the kinetic coefficient in solid-liquid systems, Acta Mater. 47 (1999) 3181.
[25] C.J. Tymczak, J.R. Ray, Asymmetric crystallization and melting kinetics in sodium a molecular-dynamics study, Phys. Rev. Lett. 64 (11) (1990) 1278–1281.
[26] J.J. Hoyt, M. Asta, D.Y. Sun, Molecular dynamics simulations of the crystal-melt interfacial free energy and mobility in Mo and V, Philos. Mag. 86 (24) (2006) 3651–3664.
[27] J.J. Hoyt, M. Asta, Atomistic computation of liquid diffusivity, solid-liquid interfacial free energy, and kinetic coefficient in Au and Ag, Phys. Rev. B 65 (2002), 214106.
[28] D.Y. Sun, M. Asta, J.J. Hoyt, Crystal-melt interfacial free energies and mobilities in fcc and bcc Fe, Phys. Rev. B 69 (2004), 174103.
[29] T. Fang, L. Wang, Y. Qi, Molecular dynamics simulation of crystal growth of undercooled liquid Co, Physica B. 423 (2013) 6.
[30] T. Fang, L. Wang, Y. Qi, Solid-liquid interface growth of $Cu_{50}Ni_{50}$ under deep undercoolings, Phys. Chem. Liquids 52 (2013) 342.
[31] Y. Ashkenazy, R.S. Averback, Kinetic stages in the crystallization of deeply undercooled body-centered-cubic and face-centered-cubic metals, Acta Materialia 58 (2010) 524.
[32] R. Ramakrishnan, R. Sankarasubramanian, Crystal-melt kinetic coefficients of Ni_3Al, Acta Mater. 127 (2017) 25.
[33] W.L. Chan, R.S. Averback, D.G. Cahill, Y. Ashkenazy, Solidification velocities in deeply undercooled silver, Phys. Rev. Lett. 102 (2009), 095701.
[34] X.Q. Yan, Y.J. Lu, Mechanism of abnormally slow crystal growth of CuZr alloy, J. Chem. Phys. 143 (2015), 164503.
[35] Q. Yang, H. Liu, H. Peng, Crystal growth in deeply undercooled Ni50Al50: Signature of the ordering sequence at the interface, Chem. Phys. 154 (2021), 194503.
[36] A. Schottelius, et al., Crystal growth rates in supercooled atomic liquid mixtures, Nature Materials 19 (2020) 512.
[37] C.C. Prado, J.P. Rino, An interaction potential for zinc selenide: a molecular dynamics study, J. Appl. Phys 129 (2021), 055104.
[38] L. Separdar, J.P. Rino, E.D. Zanotto, Molecular dynamics simulations of spontaneous and seeded nucleation and theoretical calculations for zinc selenide, J. Comp. Material Science 187 (2021), 110124.
[39] G. Grebe, G. Roussos, H.-J. Schulz, Cr2+ excitation levels in ZnSe and ZnS, J. Phys. C: Solid state Phys. 9 (24) (1976) 4511–4516.
[40] S. Guha, Zinc Selenide, Encyclopedia Mater.: Sci. Technol. (2011) 9894–9897, https://doi.org/10.1016/B0-08-043152-6/01791-5. ISBN: 978-0-08-043152-9.
[41] S. Adachi, T. Taguchi, Optical properties of ZnSe, Phys. Rev. B 43 (12) (1991) 9569–9577.
[42] I. Kikuma, M. Furukoshi, Direct observation of the 3C–2H transformation in ZnSe by high-temperature X-ray diffraction, J. Crystal Growth 71 (1985) 136.
[43] S.u. Ching-Hua, Y.-G. Sha, Growth of wide band gap II-VI compound semiconductors by physical vapor transport, Current Topics in Crystal Growth Res. 2 (1995) 40188–40194.
[44] R.J.P. Eder, E.K. Schmitt, J. Grill, S. Radl, H. Gruber-Woelfler, J.G. Khinast, Seed loading effects on the mean crystal size of acetylsalicyclic acid in a continuous-flow crystallization device, Cryst Res Technol 46 (2011) 227.
[45] B. Loï Mi Lung-Somarriba, M. Moscosa-Santillan, C. Porte, A. Delacroix, Effect of seeded surface area on crystal size distribution in glycine batch cooling crystallization: a seeding methodology, J. Crystal Growth 270 (3-4) (2004) 624–632.
[46] S. Jungblut, C.h. Dellago, Crystallization on prestructured seeds, Phys. Rev. E 87 (2013), 012305.
[47] D. Suh, K. Yasuoka, Nanoparticle growth analysis by molecular dynamics: spherical seed, J. Phys. Chem. B 115 (36) (2011) 10631–10645.
[48] F. Lodesani, M.C. Menziani, K. Maeda, et al., Disclosing crystal nucleation mechanism in lithium disilicate glass through molecular dynamics simulations and free-energy calculations, Sci Rep 10 (2020) 17867.
[49] M.G. Lioliou, Ch. A. Paraskeva, P.G. Koutsoukos, Al. C. Payatakes, Heterogeneous nucleation and growth of calcium carbonate on calcite and quartz, J. Colloid Interface Sci. 308 (2007) 421, https://doi.org/10.1016/j.jcis.2006.12.045.
[50] L. Separdar, J.P. Rino, E.D. Zanotto, Unveiling nucleation dynamics by seeded and spontaneous crystallization in supercooled liquids, J. Comp. Material Science 199 (2021), 110802.
[51] K.A. JACKSON, in: R.H. Doremus, B.W. Roberts, D. Turnbull (Eds.), Growth and Perfection of Crystals, Wiley, New York, 1958, pp. 339–349.
[52] W.K. Burton, N. Cabrera, F.C. Frank, The growth of crystals and the equilibrium structure of their surfaces, Proc. R. Soc. Lond. A 243 (1951) 299.
[53] D.R. Uhlmann, Crystal growth in glass-forming systems: a ten-year perspective, nucleation and crystallization in glasses, Advances in Ceramics, American Ceramic Society 20 (1982) 20.
[54] L.L. Burgner, M.C. Weinberg, Crystal growth mechanisms in inorganic glasses, Phys. Chem. Glasses 42 (2001) 184.
[55] K.F. Kelton, Crystal Nucleation in liquids and glasses, Solid State Phys. 45 (1991) 75.
[56] S.J. Plimpton, Fast parallel algorithms for short-range molecular dynamics, Comp. Phys. 117 (1995) 1.
[57] P.J. Steinhardt, D.R. Nelson, M. Ronchetti, Bond-orientational order in liquids and glasses, Phys. Rev. B 28 (1983) 784.
[58] P.R. ten Wolde, D. Frenkel, Homogeneous nucleation and the Ostwald step rule, Chem. Phys. 1 (1999) 2191.
[59] K.A. Jackson, D.R. Uhlmann, J.D. Hunt, On the nature of crystal growth from the melt, J. Crys. Growth 1 (1967) 1.
[60] J. Jiusti, E.D. Zanotto, D.R. Cassar, M.R.B. Andreeta, Viscosity and liquidus-based predictor of glass-forming ability of oxide glasses, J. American Ceram. Soci. 103 (2020) 921.
[61] J. Ovrava, L. Greer, Fast and slow growth kinetics in glass-forming melts, J. Chem. Phys. 140 (2014), 214504.
[62] S. Yau, P. Vekilov, Direct observation of nucleus structure and nucleation pathways in apoferritin crystallization, J. Am. Chem. Soc. 123 (2001) 1080.
[63] P. Davide Cozzoli, L. Manna, M. Lucia Curri, S. Kudera, C. Giannini, M. Striccoli, A. Agostiano, Shap and phase control of colloidal ZnSe Nanocrystals, Chem. Mater. 17 (2005) 1296, https://doi.org/10.1021/cm047874v.
[64] C.Y. Yeh, Z.W. Lu, S. Foyen, A. Zunger, Zinc-blende–wurtzite polytypism in semiconductors Phys, Rev. B 46 (1992) 10086.
[65] J. Schindelin, I. Arganda-Carreras, E. Frise, V. Kaynig, M. Longair, T. Pietzsch, S. Preibisch, C. Rueden, S. Saalfeld, B. Schmid, J.Y. Tinevez, D.J. White, V. Hartenstein, K. Eliceiri, P. Tomancak, A. Cardona, Fiji: an open-source platform for biological-image analysis, Nat. Methods 9 (2012) 676.
[66] S.C.C. Prado, J.P. Rino, E.D. Zanotto, Successful test of the classical nucleation theory by molecular dynamic simulations of BaS, Computational Materials Science 161 (2019) 99–106.
[67] J.C.E.L. Wang, Y. Cai, H.A. Wu, S.N. Luo, Crystallization in supercooled liquid Cu: homogeneous nucleation and growth, J. Chem. Phys. 142 (2015), 064704.
[68] L. Yu, Nucleation of one polymorph by another, J. Am. Chem. Soc. 125 (21) (2003) 6380–6381.